EPJ manuscript No.
(will be inserted by the editor)

Radiative corrections beyond the ultra relativistic limit in unpolarized ep elastic and Møller scatterings for the PRad Experiment at Jefferson Laboratory

I. Akushevich[1], H. Gao[1], A. Ilyichev[2], and M. Meziane[1]

[1] Duke University, Durham, NC 27708, USA
[2] National Center of Particle and High Energy Physics, 220088 Minsk, Belarus

Received: date / Revised version: date

Abstract. The clear 7σ discrepancy between measurements of the proton charge radius from muonic hydrogen Lamb shifts and those from hydrogen Lamb shift and electron scattering lead to both intense theoretical and experimental efforts to understand and explain this difference. In this regard, a new experiment (PRad) based on unpolarized ep elastic scattering cross section measurements normalized to Møller scattering is underway at Jefferson Laboratory to extract the proton charge radius based on new proton electric form factor down to values of momentum transfer squared Q^2, as low as 10^{-4} $(\mathrm{GeV/c})^2$. To reach the precision of the experiment in such a small Q^2 region requires reliable knowledge of radiative corrections. In this paper, we present a complete calculation of radiative corrections for unpolarized elastic ep and Møller scatterings performed within a covariant formalism resulting in the set of explicit formulas beyond the ultra relativistic approximation ($m_e^2 \ll Q^2$), and numerical results for the kinematics of the PRad experiment.

PACS. PACS-key 13.40.Ks, 13.60.Fz, 13.88.+e, 25.30.Bf, 13.40.Gp

1 Introduction

The proton charge radius, defined as the root-mean-square charge radius, is a fundamental structure parameter of the proton. The precise knowledge of it is crucial to understand how the fundamental theory of strong interaction, quantum chromodynamics (QCD) describes the structure of the nucleon. It is also an important input to quantum electrodynamics (QED) calculations of hydrogen Lamb shifts and fine structure. As such precise information about this quantity will in principle also allow for high precision tests of QED. The proton charge radius has been commonly determined from electron-proton elastic scattering experiments [1,2]. However, the precision and the consistency of the proton charge radius values determined from electron scattering experiments are not at the level that such high precision tests of QED are feasible. Instead atomic physicists have been extracting the proton charge radius using precise measurements of the hydrogen Lamb shifts [3] and the state-of-the-art QED calculations [4]. Consistent results on the proton charge radius have been obtained between electron scattering and hydrogen Lamb shift measurements.

In 2010, the high precision measurement of the proton charge radius performed at PSI [5] from muonic hydrogen Lamb shift puzzled the physics community. The extracted value (0.8418±0.0007 fm) was 7σ smaller than the previous determinations obtained from reanalysis of electron-proton scattering experiments (0.895±0.018 fm) [6], and based on spectroscopy of electronic hydrogen (0.8768± 0.0069 fm) [3,7,8]. More recent result from muonic hydrogen Lamb shift measurement at PSI (0.84087±0.0005 fm) [9] confirmed this disagreement. Furthermore, additional extractions of the proton charge radius from electron scattering at Mainz (0.879±0.008 fm) [10], from the Jefferson Laboratory analysis which includes the new constraint from the proton form factor ratio obtained with recoil polarization technique (0.875±0.010 fm) [11], and from a Bayesian inference approach [12] are also in good agreement with those "electronic" determinations. Recent reanalyses of the Mainz data using a fit function based on a conformal mapping [13] and a dispersive framework [14] found results consistent with the muonic hydrogen measurements.

This discrepancy between the experimental data led to intense theoretical efforts aiming at explaining this disagreement by including a novel two-photon exchange effect [15], an unexpected proton structure [16–18], atomic physics corrections [19], model independent calculations of the muonic hydrogen Lamb shift [20] and others. New physics such as new scalar and vector particles that couple muons to protons [21–23] and dark photons [24,25] has also been proposed to explain this discrepancy. The reliability of truncated Taylor series expansion fits has also

been investigated [26]. The observation of a smaller proton radius from muonic hydrogen compared to that from electronic hydrogen, is still to date an open question.

The root-mean-square (rms) charge radius of the proton is the slope of the Taylor expansion of the electric form factor, which can be determined from elastic electron-proton scattering [27,28], at momentum transfer $Q^2 \to 0$:

$$\langle r^2 \rangle = -6 \frac{dG_E^p(Q^2)}{dQ^2}\bigg|_{Q^2=0} \tag{1}$$

From this expression we clearly see the significance of measurement of the proton electric form factor at very low Q^2. An independent measurement (the PRad experiment) of the proton charge radius from unpolarized elastic ep scattering using a magnetic spectrometer free method was proposed at Jefferson Laboratory [29]. The incident beam electrons will scatter off a windowless cryocooled hydrogen gas flow target and will be detected with the high resolution PrimEx HYCAL calorimeter [30]. The ep cross sections will be normalized to the well known Møller cross sections measured simultaneously within the same detector acceptance allowing to reach an unprecedented subpercent precision of the charge radius in electron scattering experiments in an essentially model independent way. This novel technique makes possible the extraction of the charge radius at very forward angles and thus very low values of Q^2 down to 10^{-4} GeV^2 compared to the lowest $Q^2 = 0.01$ GeV^2 of [10]. At Mainz, the technique of initial state radiation in ep elastic scattering was used recently to reach a Q^2 value of 10^{-4} GeV^2 [31]. A proposed experiment at PSI [32] will measure r_p down to $Q^2 = 4 \times 10^{-3}$ GeV^2 from μp elastic scattering.

In order to reach such a precision, in addition to a tight control of systematic uncertainties and a precise knowledge of backgrounds associated with the experiment, a careful calculation of radiative corrections (RC) is necessary. Since in the PRad experiment the ep and Møller cross sections will be measured separately, we need to perform two distinct calculations for the ep and Møller processes. Until now, all available calculations of radiative corrections in elastic ep [33,34] and Møller [35] scatterings were carried out using the ultra relativistic approximation (URA), where the electron mass squared $m_e^2 \ll Q^2$, and had been neglected. The explicit expressions without URA for one-loop (*i.e.* vertex, self-energies and two photon exchange) contributions to Møller scatterings are presented in [36], however the contribution from hard photon emission was not considered.

In sect. 2 and 3, we present a complete calculation of the ep and Møller radiative corrections within a covariant formalism beyond the URA. For the first time, analytical expressions were obtained for the Møller box diagrams and for the infrared divergent contribution of the bremstrahlung process without any approximation. It is important to note that names given to different contributions vary section to section. This is to match the names given in previous papers ([33] for ep and [35] for Møller), where the results are given in the URA, for an easier comparison. In section 4 we show numerical results of the total ep and Møller radiative corrections over a wide kinematical range relevant to the PRad experiment.

2 Radiative Corrections to the ep Elastic Scattering Unpolarized Cross Section

In this paper, all the expressions for the cross section and radiative corrections are presented within the covariant formalism developed by Bardin and Shumeiko [39]. It allows to obtain a general result independent of any unphysical parameter like a cut-off parameter distinguishing the regions of soft and hard photon emission, while canceling out the infrared divergences. We consider the unpolarized electron-proton elastic scattering:

$$e(k_1) + N(p_1) \longrightarrow e'(k_2) + N(p_2) \tag{2}$$

with k_1 (p_1) and k_2 (p_2) being the initial and final 4-momenta of the electron (proton). The 4-momentum of the virtual photon is given by $q = k_1 - k_2$. The Born Cross section of this process is given by:

$$\frac{d\sigma_0}{dQ^2} = \frac{2\alpha^2\pi}{\lambda_S Q^4} \sum_i \theta_B^i \mathcal{F}_i^0 \tag{3}$$

where:

$$\lambda_S = S^2 - 4m^2M^2 \tag{4}$$
$$\mathcal{F}_1^0 = (F_1(Q^2) + F_2(Q^2))^2 \tag{5}$$
$$\mathcal{F}_2^0 = F_1^2(Q^2) + F_2^2(Q^2)\frac{Q^2}{4M^2} \tag{6}$$

and

$$\theta_B^1 = Q^2 - 2m^2 \tag{7}$$
$$\theta_B^2 = \frac{1}{2M^2}(SX - M^2Q^2) \tag{8}$$

with the 4-momentum transfer $Q^2 = -q^2 = -(k_1 - k_2)^2$, $S = 2k_1 \cdot p_1$, $X = 2k_2 \cdot p_1 = S - Q^2$, m and M are the masses of the electron and proton, respectively. The Feynamn diagrams of interest for the calculation of radiative corrections are shown in fig. 1. In addition to the Born process (a), the vertex correction (b), the vacuum polarization (c), and the bremsstrahlung (d) and (e) are taken into account.

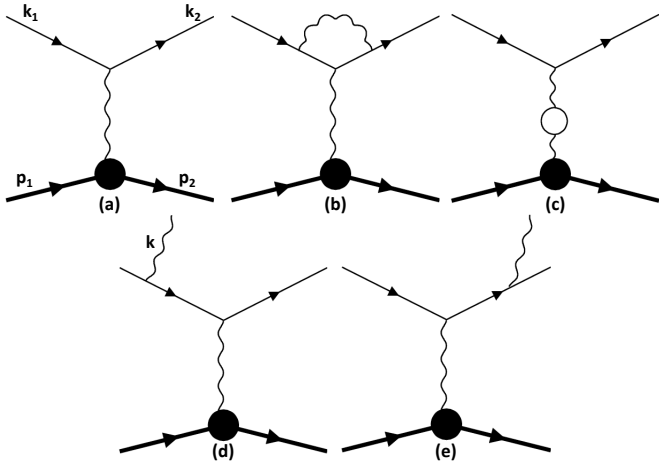

Fig. 1: Feynman diagrams contributing to the Born and radiative correction cross sections for ep elastic scattering.

The cross section of the bremsstrahlung process:

$$e(k_1) + N(p_1) \longrightarrow e'(k_2) + N(p_2) + \gamma(k) \tag{9}$$

where k is the 4-momentum of the emitted hard photon, is given by:

$$d\sigma_r = \frac{1}{2\sqrt{\lambda_S}} \mathcal{M}_r^2 d\Gamma_r \tag{10}$$

The phase space can be expressed in terms of the inelasticity $v = \Lambda^2 - M^2$, ($\Lambda = k_1 + p_1 - k_2$), $\tau = k \cdot q / k \cdot p_1$ and the angle ϕ between the planes ($\mathbf{q}$,$\mathbf{k}$) and ($\mathbf{k}_1$,$\mathbf{k}_2$):

$$d\Gamma_r = \frac{dQ^2}{4(2\pi)^4\sqrt{\lambda_S}} \int\limits_0^{v_{max}} \frac{dv}{4\sqrt{\lambda_Y}} \int\limits_{\tau_{min}}^{\tau_{max}} d\tau \frac{v}{(1+\tau)^2} \int\limits_0^{2\pi} d\phi \tag{11}$$

where $\lambda_Y = (v+Q^2)^2 + 4M^2Q^2$. The limits of integrations are given by:

$$v_{max} = \frac{2Q^2(\lambda_S - Q^2(S + m^2 + M^2))}{Q^2(S+2m^2) + \sqrt{Q^2\lambda_S(Q^2+4m^2)}} \tag{12}$$

$$\tau_{max,min} = \frac{1}{2M^2}(v + Q^2 \pm \sqrt{\lambda_Y}) \tag{13}$$

Usually an experimental cut is applied to inelasticity v. In this case the value of this cut should be used for v_{max} instead of (12). The matrix element squared $\mathcal{M}_r^2$ of the bremsstrahlung process is given by the product of the radiative leptonic tensor $L^r_{\mu\nu}$ by the hadronic tensor $W_{\mu\nu}$:

$$\mathcal{M}_r^2 = \frac{e^6}{t^2} L^r_{\mu\nu} W_{\mu\nu} = \frac{e^6}{t^2} L^r_{\mu\nu} \sum_{i=1}^{2} w^i_{\mu\nu} \mathcal{F}_i. \tag{14}$$

The structure functions $\mathcal{F}_{1,2}$ can be written via $\mathcal{F}^0_{1,2}$ by the following replacement of the argument $Q^2 \to Q^2 + \tau v/(1+\tau)$. The contractions of the two tensors can be expanded in powers of $R = 2p_1 \cdot k = v/(1+\tau)$:

$$L^r_{\mu\nu} w^i_{\mu\nu} = -4\pi\sqrt{\lambda_Y} \sum_{j=1}^{3} R^j \theta_{ij} \tag{15}$$

with: $w^1_{\mu\nu} = -g_{\mu\nu}$, $w^2_{\mu\nu} = p_{1\mu}p_{1\nu}/M^2$. The functions θ_{ij} are given by:

$$\theta_{11} = 4(Q^2 - 2m^2)F_{IR} \tag{16}$$

$$\theta_{12} = 4\tau F_{IR} \tag{17}$$

$$\theta_{13} = -4F - 2\tau^2 F_d \tag{18}$$

$$\theta_{21} = \frac{2}{M^2}(SX - M^2Q^2)F_{IR} \tag{19}$$

$$\theta_{22} = \frac{1}{2M^2}(2(S+X)F_{2-} + (S^2 - X^2)F_{1+} \tag{20}$$

$$+2(S - X - 2M^2\tau)F_{IR} - \tau(S+X)^2 F_d) \tag{21}$$

$$\theta_{23} = \frac{1}{2M^2}(4M^2F + (4m^2 + 2M^2\tau^2$$

$$-(S-X)\tau)F_d - (S+X)F_{1+}) \tag{22}$$

where:

$$F_{IR} = F_{2+} - (Q^2 + 2m^2)F_d, \quad F_d = \frac{F}{z_1 z_2}$$

$$F_{2\pm} = Fm^2\left(\frac{1}{z_2^2} \pm \frac{1}{z_1^2}\right), \quad F_{1+} = \frac{F}{z_1} + \frac{F}{z_2}$$

$$F = \frac{1}{2\pi\sqrt{\lambda_Y}}$$

The propagators are given by:

$$z_1 = \frac{1}{\lambda_Y}\left[Q^2(S+X) + \tau(S(S-X) + 2M^2Q^2)\right. \tag{23}$$

$$\left. -2M\sqrt{\lambda_z}\cos\phi\right]$$

$$z_2 = \frac{1}{\lambda_Y}\left[Q^2(S+X) + \tau(S(S-X) - 2M^2Q^2)\right. \tag{24}$$

$$\left. -2M\sqrt{\lambda_z}\cos\phi\right]$$

with: $\lambda_z = (\tau - \tau_{min})(\tau_{max} - \tau)(SXQ^2 - M^2Q^4 - m^2\lambda_Y)$. To extract the infrared divergence we use the transformation:

$$\sigma_R = \sigma_R - \sigma_{IR} + \sigma_{IR} = \sigma_F + \sigma_{IR} \tag{25}$$

where σ_F is infrared divergence free (finite when $k \to 0$). We used the notation $\sigma_a \equiv d\sigma_a/dQ^2$ ($a = R,\ IR,\ F,\ etc$).

The infrared part of the cross section σ_{IR}, can be written as a sum of a soft σ_S and hard part σ_H by splitting the domain of integration over the inelaticity:

$$\sigma_{IR} = \frac{\alpha}{\pi}(\delta_S + \delta_H)\sigma_0 \tag{26}$$

$\delta_H + \delta_S$ can be written as [39]:

$$\delta_H + \delta_S = 2\left(Q_m^2 L_m - 1\right)\ln\frac{v_{max}}{M\lambda} \tag{27}$$

$$+\frac{1}{2}(SL_S + (S - Q^2)L_X^0) + S_\phi(Q_m^2, \lambda_m, a, b)$$

with λ the infinitesimal photon mass and

$$Q_m^2 = Q^2 + 2m^2 \tag{28}$$
$$L_m = \frac{1}{\sqrt{\lambda_m}} \ln \frac{\sqrt{\lambda_m} + Q^2}{\sqrt{\lambda_m} - Q^2} \tag{29}$$
$$\lambda_m = Q^4 + 4m^2Q^2 \tag{30}$$
$$L_S = \frac{1}{\sqrt{\lambda_S}} \ln \frac{S + \sqrt{\lambda_S}}{S - \sqrt{\lambda_S}} \tag{31}$$
$$L_X^0 = \frac{1}{\sqrt{\lambda_X^0}} \ln \frac{S - Q^2 + \sqrt{\lambda_X^0}}{S - Q^2 - \sqrt{\lambda_X^0}} \tag{32}$$
$$\lambda_X^0 = (S - Q^2)^2 - 4m^2M^2 \tag{33}$$
$$a = \frac{1}{2M^2}(S(S - Q^2) - 2M^2(Q^2 - 2m^2)) \tag{34}$$
$$b = \frac{1}{M^2}(Q^2(S(S - Q^2) - M^2Q^2) - m^2Q^2(Q^2 + 4M^2)) \tag{35}$$

The function $S_\phi(s, \lambda, a, b)$ is given by:

$$S_\phi(s, \lambda, a, b) = \frac{s}{2\sqrt{\lambda}} \sum_{i=1}^{2} (-1)^i \sum_{j=1}^{4} \delta_j \sum_{k=1}^{2} \left[\Phi\left(\frac{\gamma_i - \gamma}{\gamma_i - \gamma_k^j} \right) + \Phi\left(\frac{\gamma + (-1)^i}{\gamma_k^j + (-1)^i} \right) \right] \Bigg|_{\gamma_1}^{\gamma_u} \tag{36}$$

where:

$$a_j = s - \delta_j\sqrt{\lambda}, \quad D = (s + a)(\lambda a - sb) + \frac{1}{4}(\lambda + b)^2$$
$$\delta_j = (1, 1, -1, -1), \quad \gamma_{1,2} = \mp\frac{\sqrt{b} \mp \sqrt{\lambda}}{b - \lambda}$$
$$\gamma_{1,2}^j = -\frac{a_j\sqrt{b} \pm \sqrt{ba_j^2 + \tau_j^2}}{\tau_j}, \quad \gamma_u \frac{\sqrt{b + \lambda} - \sqrt{b}}{\sqrt{\lambda}}$$
$$\tau_j = -a\sqrt{\lambda} + \frac{1}{2}\delta_j(b - \lambda) + (-1)^j\sqrt{D}$$

The function $\Phi(x)$ is the Spence function. To cancel the infrared divergence we need to add the standard vertex correction contribution δ_{vert}. Beyond the URA it is given by:

$$\delta_{vert} = 2\left(Q_m^2 L_m - 1\right) \ln \frac{\lambda}{m} + \left(\frac{3}{2}Q^2 + 4m^2\right) L_m - 2 - \frac{Q_m^2}{\sqrt{\lambda_m}} \left(\frac{1}{2}\lambda_m L_m^2 + 2\Phi\left(\frac{2\sqrt{\lambda_m}}{Q^2 + \sqrt{\lambda_m}} \right) - \frac{\pi^2}{2} \right) \tag{37}$$

The correction must vanish in the limit $Q^2 \to 0$ because of the charge renormalization. Indeed, the δ_{vert} is proportional to Q^2 in this limit:

$$\delta_{vert} = \frac{Q^2}{12m^2}\left(3 + 8\log\frac{\lambda}{m}\right) \tag{38}$$

Adding the different contributions, we clearly see that the infrared divergence cancels out explicitly. The contribution of the anomalous magnetic moment reads:

$$\sigma_{AMM} = \frac{\alpha^3 m^2 L_m (12M^2\mathcal{F}_1^0 - (Q^2 + 4M^2)\mathcal{F}_2^0)}{2M^2Q^2\lambda_S} \tag{39}$$

The final expression for the cross section beyond the URA is given by:

$$\sigma = \sigma_0(1 + \frac{\alpha}{\pi}(\delta_{VR} + \delta_{vac} - \delta_{inf}))e^{\frac{\alpha}{\pi}\delta_{inf}} + \sigma_{AMM} + \sigma_F \tag{40}$$

with:

$$\delta_{VR} = 2\left(Q_m^2 L_m - 1\right) \ln\left(\frac{v_{max}}{mM}\right) + \frac{1}{2}(SL_S + (S - Q^2)L_X^0) + S_\phi(Q_m^2, \lambda_m, a, b) + \left(\frac{3}{2}Q^2 + 4m^2\right) L_m - 2 - \frac{Q_m^2}{\sqrt{\lambda_m}} \times \left(\frac{1}{2}\lambda_m L_m^2 + 2\Phi\left(\frac{2\sqrt{\lambda_m}}{Q^2 + \sqrt{\lambda_m}} \right) - \frac{\pi^2}{2} \right) \tag{41}$$

$$\delta_{vac} = \sum_{i=e,\mu,\tau} \left[\frac{2}{3}(Q^2 + 2m_i^2)L_m^i - \frac{10}{9} + \frac{8m_i^2}{3Q^2}(1 - 2m_i^2 L_m^i) \right] \tag{42}$$

$$\delta_{inf} = \left(Q_m^2 L_m - 1\right) \ln\left(\frac{v_{max}^2}{S(S - Q^2)} \right) \tag{43}$$

$$\sigma_F = -\frac{\alpha^3}{2\lambda_S} \int_0^{v_{max}} dv \int_{\tau_{min}}^{\tau_{max}} \frac{d\tau}{1 + \tau} \int_0^{2\pi} d\phi \times \sum_{i,j} \left(R^{j-2}\theta_{ij} \frac{\mathcal{F}_i}{(Q^2 + R\tau)^2} - 4F_{IR}\theta_i^B \frac{\mathcal{F}_i^0}{RQ^4} \right) \tag{44}$$

The δ_{inf} term is to account for multi-photon emission when $Q^2 \to 0$. More detail about this exponentiation procedure can by found in [40]. δ_{vac} is the vacuum polarization correction, which includes the vacuum polarization by e, μ and τ charged leptons. The correction is small in the region of small Q^2 because it is exactly zero for $Q^2 \to 0$ due to the mass renormalization. The first non-vanishing term is

$$\delta_{vac} = \frac{2Q^2}{15} \sum_{i=e,\mu,\tau} \frac{1}{m_i^2}. \tag{45}$$

The vacuum polarization by hadrons can be considered in the same way. Note that the approach traditionally used for the vacuum polarization by hadrons involving the data on process $e^+e^- \to$ hadrons via dispersion relations is not used here because respective parameterization of [42] ($\delta_{vac}^h \cong A + B\ln(1 + C|t|)$) does not provide the correct behavior for small $Q^2 = |t|$.

3 Radiative Corrections to Møller scattering

We consider the unpolarized Møller scattering:

$$e(k_1) + e(p_1) \longrightarrow e(k_2) + e(p_2) \tag{46}$$

with k_1 (p_1) and k_2 (p_2) the initial and final 4-momenta of the beam (target) electron of mass m. The Mandelstam variables associated with this process can be written in the standard way:

$$s = (k_1 + p_1)^2,\ t = (k_1 - k_2)^2 = -Q^2,\ u_0 = (k_2 - p_1)^2 \tag{47}$$

and $s + t + u_0 = 4m^2$. It is also usefull to define the variables:

$$\xi_s = \frac{\sqrt{s - 4m^2}}{\sqrt{s}},\ \xi_t = \frac{\sqrt{4m^2 - t}}{\sqrt{-t}},\ \xi_{u_0} = \frac{\sqrt{4m^2 - u_0}}{\sqrt{-u_0}} \tag{48}$$

The Born cross section (figs. 2a, 2b) of the Møller process beyond the URA is represented as a sum of the contributions of the t and u channels,

$$\sigma_0 = \sigma_0^t + \sigma_0^{u_0} \tag{49}$$

where

$$\sigma_0^t = \frac{2\pi\alpha^2}{st^2}\left[\frac{u_0^2}{4s\xi_s^2}\left(4\xi_{u0}^4 - (1-\xi_{u0}^2)^2\left(2 + \frac{t}{u_0}\right)\right) - \frac{s^2\xi_s^4}{u_0}\right] \tag{50}$$

and the contribution of the u channel, $\sigma_0^{u_0}$, is obtained from σ_0^t by the substitution $t \longleftrightarrow u_0$. The cross section in t channel contains the contribution of the square of t-channel Feynman graph shown in fig. 2a and the half of the interference between graphs a) and b). The u channel cross section includes the contributions of the remaining part of the interference term (*i.e.*, the second half) and the square of the u-channel graph b). Note that $1 > \xi_s > 0$ while $\xi_{t,u_0} > 1$ and in URA, where $\xi_{s,t,u_0} \to 1$, we retrieve the expression (3) of ref. [35].

All other graphs shown in fig. 2 (*i.e.*, graphs c-k) represent radiative corrections due to loop effects and emission of the real photon. Only t-channel graphs are shown but respective u-channel diagrams are also included in the calculation. Similarly to the Born cross section, the contribution of each graph can be split into t and u channel cross sections. These cross sections contain the convolution of respective graphs (e.g., t-channel of vacuum polarization includes the convolution of graphs a) and c) and a half of interference between graphs of different channels. The interference is always symmetric with respect to $t \longleftrightarrow u_0$, so the t, u channels can be obtained from each other by this substitution.

The cross section of vacuum polarization (fig. 2c) is factorized in front of the respective Born cross section:

$$\sigma_S = \frac{\alpha}{\pi}\left(\delta_{vac}^t\sigma_0^t + \delta_{vac}^u\sigma_0^u\right) \tag{51}$$

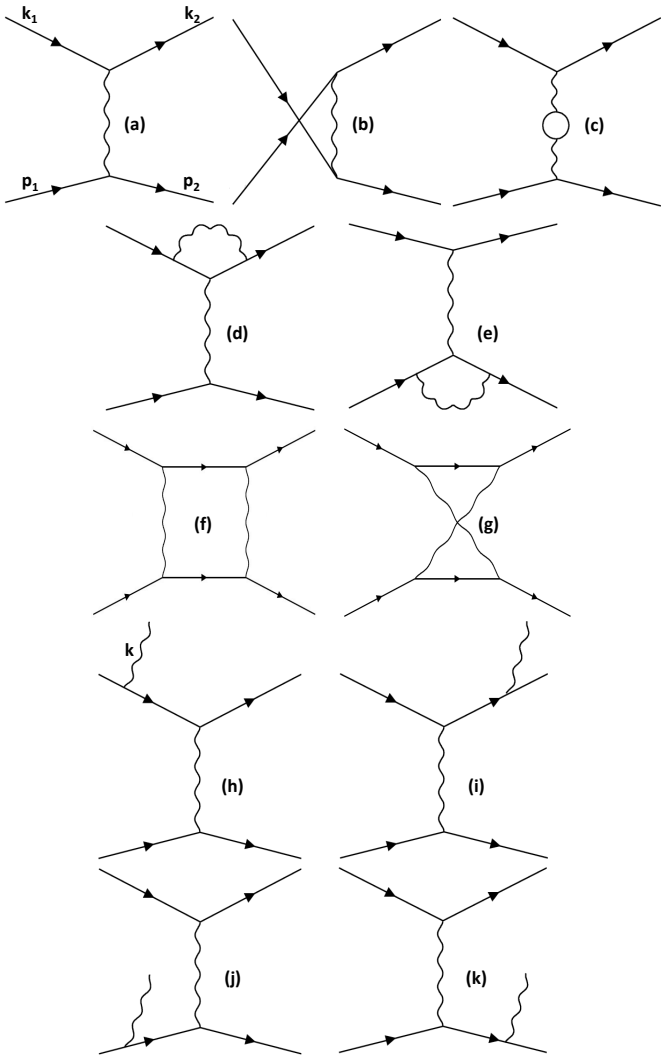

Fig. 2: Feynman diagrams contributing to the Born ((a) t- and (b) u- channels) and radiative correction (only t-channel is shown) cross sections for Møller scattering.

The correction δ_{vac}^t is defined as in Sec. 2 with the substitution $Q^2 \to -t$ and δ_{vac}^u is obtained from δ_{vac}^t by $t \longleftrightarrow u_0$.

The contribution of the vertex corrections (figs. 2d, 2e) has both factorized and non-factorized parts. The factorized part is also known as the electron form factor. This contribution is large because of the large logarithmic contributions, which contains the infrared divergence term (*i.e.*, the dependence on the photon mass). The non-factorized part is known as the anomalous magnetic moment (AMM). The cross section of AMM is proportional to m^2 and therefore it vanishes in the URA. The contributions of the vertex function are expressed as:

$$\sigma_{vert} = \frac{2\alpha}{\pi}\left(\delta_{vert}^t\sigma_0^t + \delta_{vert}^u\sigma_0^u\right) + \sigma_{AMM}^t + \sigma_{AMM}^u \tag{52}$$

The correction δ_{vert}^t and δ_{vert}^u are defined by the same formula as in eq.(37) but with $Q^2 \to -t$ and $Q^2 \to -u_0$,

respectively. The contribution of t-part of the anomalous magnetic moment is given by:

$$\sigma^t_{AMM} = -\frac{4\alpha^3}{st^2\xi_t} m^2 \log\left(\frac{\xi_t+1}{\xi_t-1}\right)\left[3\frac{s-2m^2}{u_0} + \frac{10m^2-3u_0}{s-4m^2}\right] \quad (53)$$

and $\sigma^u_{AMM} = \sigma^t_{AMM}(t \longleftrightarrow u_0)$.

The contributions of the box diagrams (figs. 2f, 2g) contain also factorized and non-factorized parts. The infrared divergence is contained in the factorized part only.

$$\sigma_B = \frac{\alpha}{2\pi}\left(\delta^t_{Box}\sigma^t_0 + \delta^u_{Box}\sigma^u_0\right) + \sigma^t_{B1} + \sigma^t_{B2} + \sigma^u_{B1} + \sigma^u_{B2}, \quad (54)$$

where

$$\delta^t_{Box} = \frac{1+\xi_s^2}{\xi_s}\left(-4\log\left[\frac{1+\xi_s}{1-\xi_s}\right]\log\frac{\lambda}{m} + \log^2\left[\frac{1+\xi_s}{1-\xi_s}\right] - 2\pi^2 + 4\mathrm{Li}_2\left[\frac{2\xi_s}{1+\xi_s}\right]\right) + \frac{1+\xi_{u_0}^2}{\xi_{u_0}}\left(4\log\left[\frac{1+\xi_{u_0}}{\xi_{u_0}-1}\right]\log\frac{\lambda}{m} - \log^2\left[\frac{1+\xi_{u_0}}{\xi_{u_0}-1}\right] + 2\log^2\left[\frac{1+\xi_{u_0}}{2\xi_{u_0}}\right] - \frac{\pi^2}{3} + 4\mathrm{Li}_2\left[\frac{\xi_{u_0}+1}{2\xi_{u_0}}\right]\right) \quad (55)$$

and the explicit expressions for σ^t_{B1} and σ^t_{B2} can be found in Appendix. Note that σ^t_{B1} and σ^t_{B2} do not have mass singularity terms $\log(m^2)$. As usual the contributions in u-channel are obtained using $t \longleftrightarrow u_0$.

All contributions to radiative corrections in Møller scattering discussed above agree exactly with the respective terms presented in eq. (2) of ref. [36]. The lowest order (Born) cross section given by the first term in $\otimes$ (*i.e.*, the term with the product symbol in the first line of eq. (2)) corresponds to our eq. (49). The vertex functions and vacuum polarization corrections represented by the terms including I and II classes are exactly the same as the contributions given by eqs. (52) and (51) of our paper. Finally, the sum of classes with direct and crossed two-photon exchange diagrams (III and IV) corresponds to our result in eq. (54) in this section.

The real photon emission process (fig. 2h-k):

$$e(k_1) + e(p_1) \longrightarrow e(k_2) + e(p_2) + \gamma(k) \quad (56)$$

requires three additional kinematical variables to describe its cross section. They are chosen as two photon angles and the inelasticity $v = (k_1+p_1-k_2)^2 - m^2$. The relation between the Mandelstam variables is generalized:

$$s + u + t = v + 4m^2, \quad (57)$$

i.e., the sum of s, t and u is not fixed by the electron mass.

The cross section of the process (56) contains the infrared divergence, therefore a procedure for its extraction and cancellation is required. We follow the approach suggested by Bardin and Shumeiko [39] based on the following transformation:

$$\sigma_R = \sigma_R - \sigma_{IR} + \sigma_{IR} = \sigma_F + \sigma_{IR} \quad (58)$$

The infrared divergence is then only contained in σ_{IR}, which has a simple analytical form. The finite part of the cross section has to be integrated over the photonic angles and the inelasticity. Two-dimensional integration over the photonic angles is performed analytically while the integration over v is carried out numerically.

$$\sigma_F = -\frac{\alpha^3}{\pi s(s-4m^2)}\int_0^{v_{max}} dv \sum_{i=1}^{10} S_i, \quad (59)$$

The upper integration limit v_{max} is defined by the kinematic restrictions or, more often, by the experimental cuts, because v can also be reconstructed using the momenta of the final particles. The integrand is defined by ten terms S_i, that are polynomial functions of s, t, u, m^2, and v. The infrared divergence is cancelled using the aforementioned procedure in eq. (58), therefore the terms S_i are finite for $v = 0$. The explicit expressions of S_i are cumbersome and not presented here. The expressions calculated within URA can be found in Appendix of [35] while their exact expressions (beyond URA) can be found in the source code of the Monte-Carlo generator MERADGEN 1.0 [43]. Note that all parts of the cross section describing the process (56) are not separated into t- and u-parts.

The infrared divergent contribution of bremsstrahlung integrated over the real photon phase space is represented as a sum of three factorized corrections:

$$\sigma_{IR} = \frac{\alpha}{\pi}(J_0 \log\frac{v_{max}}{m\lambda} + \delta_1^H + \delta_1^S)\sigma_0 \quad (60)$$

where

$$J_0 = -2\left(\frac{\xi_s^2+1}{\xi_s}\log\frac{\xi_s+1}{1-\xi_s} - \frac{\xi_t^2+1}{\xi_t}\log\frac{\xi_t+1}{\xi_t-1} - \frac{\xi_{u0}^2+1}{\xi_{u0}}\log\frac{\xi_{u0}+1}{\xi_{u0}-1} + 2\right) \quad (61)$$

The explicit expressions for δ_1^H and δ_1^S obtained without any approximation are given in Appendix. Within the URA they are reduced to the expressions (B.10) of [43]:

$$\begin{aligned}\delta_1^H = {} & \log(-\frac{t}{m^2})(\log(\frac{t^2(s+t)^2(s-v_{max})}{sv_{max}(v_{max}-t)(s+t-v_{max})^2}) + 1) \\ & -\frac{1}{2}\log^2(-\frac{t}{m^2}) + 2(-\mathrm{Li}_2(\frac{v_{max}}{s+t}) + \mathrm{Li}_2(\frac{v_{max}}{s}) \\ & -\mathrm{Li}_2(\frac{v_{max}}{t})) + \mathrm{Li}_2(\frac{s-v_{max}}{s}) - \mathrm{Li}_2(\frac{t-v_{max}}{t}) \\ & +\log(\frac{s+t}{s+t-v_{max}})\log(\frac{(s+t)(s+t-v_{max})}{t^2}) \\ & +\log(\frac{s-v_{max}}{s})\log(\frac{v_{max}-s}{t}) - \frac{1}{2}\log^2(-\frac{v_{max}}{t}) \\ & -\log^2(1-\frac{v_{max}}{t}) + \log(-\frac{v_{max}}{t}) - \frac{\pi^2}{6}\end{aligned} \quad (62)$$

and

$$\delta_1^S = 1 - \left(\log\left(-\frac{t}{m^2}\right) - 1\right)\log\left(\frac{s(s+t)}{t^2}\right) + \log\left(-\frac{t}{m^2}\right)\left(3 - 2\log\left(\frac{s+t}{s}\right)\right) - \frac{5}{2}\log^2\left(-\frac{t}{m^2}\right) - \frac{1}{2}\log^2\left(\frac{s+t}{s}\right) - \frac{\pi^2}{3} \quad (63)$$

while

$$J_0^{URA} = -4\left(1 + \log\frac{m^2 s}{t u_0}\right) \quad (64)$$

The radiatively corrected cross section for Møller scattering is obtained as the sum of all the aforementioned contributions.

$$\sigma^{ee} = (1 + \frac{\alpha}{\pi}(J_0 \log\frac{v_{max}}{m^2} + \delta_1^H + \delta_1^S))\sigma_0 + \sigma_S + \sigma_{vert}^F + \sigma_B^F + \sigma_F \quad (65)$$

where upper index F in vertex and box contributions means that terms containing $\log(\lambda/m)$ are extracted from these expressions, i*.e.*, they are obtained from σ_{Vert} and σ_B by the formal substitution $\lambda \to m$. Indeed, one can see that infrared divergence is cancelled in the sum of terms proportional to $\log\lambda$ in $\delta_{vert}^{t,u}$ (see (37) and (52)), and $\delta_{Box}^{t,u}$ (see (54)), and (60).

The corrections $\delta_{vert}^{t,u}$, δ_1^H, δ_1^S as well as δ_1^{inf} contain the double logarithmic terms ($\log^2(m^2)$). However, they also cancel each other. Therefore, the largest correction for the cross section σ^{ee} contains large logarithmic terms only.

In the limit of small Q^2, the upper limit of v_{max} goes to zero. As usual this divergence is cancelled by the exponentiation procedure, which effectively accounts for the multiple soft photon emission thus resulting in:

$$\sigma^{ee} = (1 + \frac{\alpha}{\pi}(\delta_1^H + \delta_1^S))e^{\frac{\alpha}{\pi}\delta_1^{inf}}\sigma_0 + \sigma_S + \sigma_{vert}^F + \sigma_B^F + \sigma_F \quad (66)$$

where

$$\delta_1^{inf} = J_0 \log\frac{v_{max}}{m^2} \quad (67)$$

4 Numerical Results

Figure 3 shows the *ep* radiative correction $\delta^{ep} = \sigma^{ep}/\sigma_0^{ep} - 1$ (top) and Møller radiative correction $\delta^{ee} = \sigma^{ee}/\sigma_0^{ee} - 1$ (bottom) as a function of Q^2 for different values of inelasticity cut v_{cut} ($0 \le v_{cut} \le v_{max}$) with v_{max} given by eq.12 and eq.73 for the *ep* and Møller case, respectively. The results are shown for the two incident electron beam energies of the PRad experiment: 1.1 GeV (solid lines) and 2.2 GeV (dashed lines). We see that the corrections are strongly v_{cut} dependent and approach asymptotically

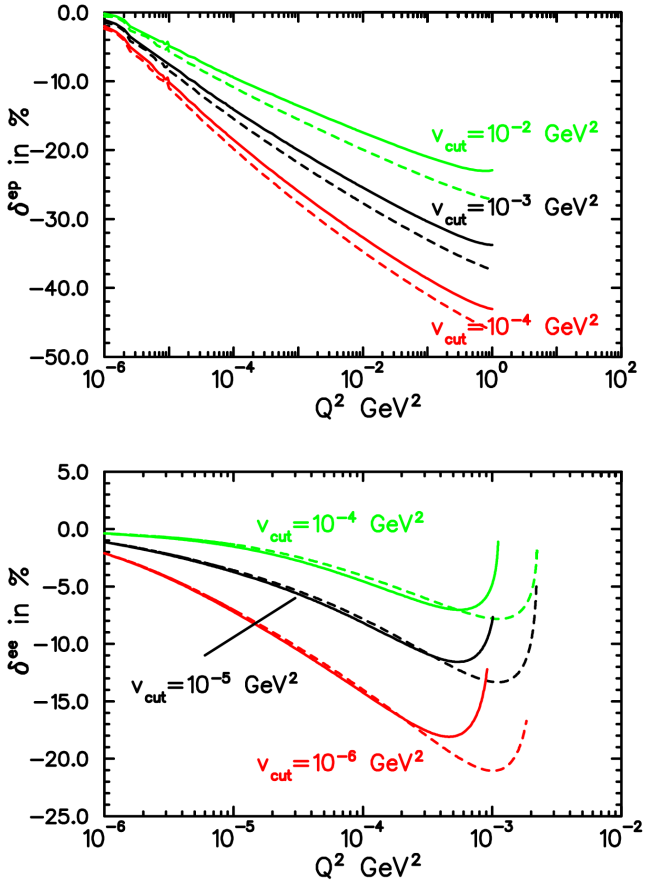

Fig. 3: *ep* (top) and Møller (bottom) radiative correction as a function of Q^2 for different values of inelasticity cut and for E_{beam}=1.1 GeV (solid lines) and E_{beam}=2.2 GeV (dashed lines). (color online)

towards 0 when Q^2 decreases 0. Furthermore, we see that the larger the inelasticity cut is, the smaller the total corrections are. Indeed for a large v_{cut} value, we cut more of the positively definite cross section of hard photon emission resulting in a decrease of the observed cross section and hence of the total radiative correction. For the kinematical settings of the PRad experiment, v_{cut} is expected to be 0.05 GeV^2 and 10^{-5} GeV^2 for *ep* and Møller scatterings, respectively. In the PRad experiment, the unpolarized *ep* elastic cross sections will be measured for $2\times10^{-4}\text{GeV}^2 \le Q^2 \le 2\times10^{-2}\text{GeV}^2$, equivalent to scattering angle in the laboratory frame $0.8^\circ \le \theta \le 3.8^\circ$ and will be normalized to the Møller cross sections within the same angular range. The radiative corrections: δ_{ep} and δ_{ee} are strongly dominated by the loop effects and soft photon emission, responsible for the strong v_{cut} dependence as expected. All the other virtual corrections and the emission of hard photon are negligible. For both processes, the total correction presents a linear behavior (with respect to the logarithmic scale of the figures) due to the leading order term $\log\left(\frac{Q^2}{m^2}\right)$.

Uncertainties in the calculation come, on one hand, from the relative accuracy of the numerical integration used to evaluate the hard photon emission σ_F for both processes. However, it has been tuned to meet and exceed the precision of the PRad experiment. On the other hand, there is a model dependence of the *ep* radiative corrections since the electromagnetic form factors are obtained from a fit. Nevertheless, all the different models agrees in the low Q^2 region making this dependence below the sensitivity of the PRad experiment.

5 Discussion and Conclusion

In this paper, a complete set of analytical expressions for electromagnetic radiative corrections to *ep* and Møller scattering obtained within a covariant formalism and beyond the ultra relativistic approximation is presented for the first time. The calculated radiative corrections are required for the proton charge radius measurements that need to be performed at very low Q^2 and therefore the URA is not appropriate. Several research groups calculated the radiative corrections to these processes but the analytical expressions presented by all of them had certain limitations preventing their direct usage for the proton radius measurement, *e.g.*, i) Akushevich et al. [33] presented the factorized part of radiative corrections to *ep*-scattering in URA, ii) Kaiser [36] and Maximon and Tjon [37] did not consider hard bremstrahlung for Møller and *ep* scattering, respectively, and iii) Shumeiko and Suarez [38] did not implement the cut-off parameter for the missing mass used in all data analyses for elastic measurements.

For the *ep* process, we presented the expressions for the so-called model independent radiative corrections including corrections due to lepton vertex functions, vacuum polarization, and emission of real photon from the leptonic line. What have not been included in the radiative correction calculations are the hadronic bremsstrahlung and the box (or two-photon exchange) diagrams. One reason is due to the fact that $M \gg m$ resulting in the hard photon emission probability from the proton to be very low. Another reason, which might be more important, is that the electromagnetic form factors are obtained from data that had not been corrected for two-photon exchange. Thus this effect is still present in the fit of form factors used for our calculation. Because of a possible double counting, it would then not be rigorous to use such form factors to perform the calculations of box diagrams and hard photon emission. Upcoming results from experiments [44–46] will provide important information about two-photon exchange effects in $e^{\pm}p$ elastic scattering, which could be used to calculate the box diagrams in the future.

For the Møller process, we presented the exact expressions of the radiative corrections including all loops and emission of additional real photon from each electron line. We find an exact agreement between our analytical expressions for the Born and one loop contributions and the ones given in [36]. However, a full comparison is not possible because the expression for cross section of soft photon emissions is not completely integrated analytically and the contribution of the hard bremsstrahlung is not considered in [36]. Our results for soft and hard photon emission in the Møller scattering are in agreement with [43].

Numerical results show that radiative corrections in *ep* and the Møller scattering could reach several dozens of percents. The radiative corrections for both processes are found strongly dependent on the inelasticity cut. Although we conclude that the radiative corrections are under control for the PRad kinematical settings, a careful analysis of systematic uncertainty due to radiative corrections will need to be performed for proton charge radius measurements.

The authors want to thank Ashot Gasparian, Mahbub Kandanker and Dipangkar Dutta for their encouragement and helpful discussions. This work was supported in part by the U. S. Department of Energy under Contract No. DE-FG02-03ER41231.

Appendix

The infrared free part of two-photon exchange contributions reads:

$$\begin{aligned}\sigma^F_{B1} = \frac{\alpha^3}{\xi_s^2 s^2 t u_0}\Bigg[&\frac{1}{12\xi_s t}((\xi_s^2+1)(\xi_s^4-6\xi_s^2-3)s^2t\\
&-2\xi_s^2(\xi_s^2+1)^3s^3-12\xi_s^2st^2-4t^3)(4\pi^2\\
&+3\log^2(\frac{\xi_s+1}{1-\xi_s})-6\log^2(\frac{\xi_s+1}{2\xi_s})\\
&-12\mathrm{Li}_2(\frac{\xi_s-1}{2\xi_s})-6\log(\frac{\xi_s+1}{1-\xi_s})\log(-\frac{\xi_s^2 s}{t}))\\
&+\frac{1}{12\xi_t^3 t}(\xi_t^2(\xi_t^2-3)(3\xi_t^2+1)t^3-2(3\xi_t^6+2\xi_t^4\\
&+10\xi_t^2-1)t^2u_0-4(5\xi_t^4+4\xi_t^2-1)tu_0^2\\
&-16\xi_t^2u_0^3)(4\pi^2-6\log^2(\frac{\xi_t+1}{2})\\
&+3\log^2(\frac{\xi_t+1}{\xi_t-1})-12\mathrm{Li}_2(\frac{1-\xi_t}{2}))\\
&+\frac{1}{\xi_s}\log(\frac{\xi_s+1}{1-\xi_s})(\xi_s^2 s+t)(\xi_s^2(\xi_s^2+1)s\\
&-2(\xi_s^2-2)t)+\log\left(\frac{1}{4}(\xi_t^2-1)\right)\big(2t^2\\
&-(\xi_s^4+\xi_s^2)s^2+(3\xi_s^2-1)st-\frac{2s(t+2u_0)}{\xi_t^2}\right)\Bigg]\end{aligned} \quad (68)$$

$$\sigma^F_{B2} = \frac{\alpha^3}{\xi_s^2 s^2 t u_0}\Bigg[\frac{1}{12\xi_{u_0} t}(4t^3 - 2(\xi^4_{u_0} - 6\xi^2_{u_0} - 1)t^2 u_0 + (-\xi^6_{u_0} + \xi^4_{u_0} + 9\xi^2_{u_0} + 7)t u_0^2 + 2(\xi^2_{u_0} + 1)^3 u_0^3) + (3\log^2(\frac{\xi_{u_0}+1}{\xi_{u_0}-1})(-6\log^2(\frac{\xi_{u_0}-1}{2\xi_{u_0}}) - 12\mathrm{Li}_2(\frac{\xi_{u_0}+1}{2\xi_{u_0}}) + 6\log(\frac{\xi_{u_0}+1}{\xi_{u_0}-1})\log(\frac{\xi^2_{u_0}u_0}{t}) + \pi^2)\frac{1}{12\xi_t^3 t}(\xi_t^2(-\xi_t^4 + 2\xi_t^2 + 3)t^3 + 2(\xi_t^6 - 4\xi_t^4 + 8\xi_t^2 + 1)t^2 u_0 + 4(3\xi_t^4 + 1)t u_0^2 + 16\xi_t^2 u^3) \times(-6\log^2(\frac{\xi_t+1}{2}) + 3\log^2(\frac{\xi_t+1}{\xi_t-1}) - 12\mathrm{Li}_2(\frac{1-\xi_t}{2}) + 4\pi^2) + \log(\frac{1}{4}(\xi_t^2-1)) \times(\frac{2u_0(\xi_t^2 t + t + 2u_0)}{\xi_t^2} + (t-u_0)(2t + \xi^2_{u_0}u_0 + u_0)) - \frac{1}{\xi_{u_0}}\log(\frac{\xi_{u_0}+1}{\xi_{u_0}-1})(\xi^2_{u_0}(t-u_0) - 2t)(2t + \xi^2_{u_0}u_0 + u_0)\Bigg] \quad (69)$$

The explicit expressions for δ_1^H and δ_1^S reads:

$$\delta_1^H = \log\left(1 + \frac{v_{max}}{m^2}\right) + H(s) - H(t) + \frac{\xi^2_{u0}+1}{2\xi_{u0}} \times\Bigg[\mathrm{Li}_2\left(\frac{4\xi_{u0}}{(\xi_{u0}+1)^2}\right) - \mathrm{Li}_2\left(-\frac{4\xi_{u0}}{(\xi_{u0}-1)^2}\right) - 2\mathrm{Li}_2\left(\frac{2\xi_{u0}}{\xi_{u0}-1}\right) + 2\mathrm{Li}_2\left(\frac{2\xi_{u0}}{\xi_{u0}+1}\right) + \mathrm{Li}_2\left(\frac{2(z_{u1}-1)\xi_{u0}}{(\xi_{u0}-1)^2}\right) + \mathrm{Li}_2\left(-\frac{2(z_{u1}+1)\xi_{u0}}{(\xi_{u0}-1)^2}\right) - \mathrm{Li}_2\left(-\frac{2(z_{u1}-1)\xi_{u0}}{(\xi_{u0}+1)^2}\right) - \mathrm{Li}_2\left(\frac{2(z_{u1}+1)\xi_{u0}}{(\xi_{u0}+1)^2}\right) + 2\mathrm{Li}_2\left(-\frac{(z_{u2}-1)\xi_{u0}}{\xi_{u0}-1}\right) + 2\mathrm{Li}_2\left(\frac{(z_{u2}+1)\xi_{u0}}{\xi_{u0}-1}\right) - 2\mathrm{Li}_2\left(\frac{(z_{u2}+1)\xi_{u0}}{\xi_{u0}+1}\right) - 2\mathrm{Li}_2\left(\frac{(1-z_{u2})\xi_{u0}}{\xi_{u0}+1}\right) + 2\log\left(\frac{\xi_{u0}+1}{\xi_{u0}-1}\right)\log\left(\frac{\xi^2_{u0}z^2_{u2}-1}{\xi^2_{u0}-1}\right)\Bigg] \quad (70)$$

$$\delta_1^S = \frac{(\xi_s^2+1)}{2\xi_s}\Bigg[\log^2\left(\frac{\xi_s+1}{1-\xi_s}\right) + \log\left(\frac{\xi_s+1}{1-\xi_s}\right) + \mathrm{Li}_2\left(\frac{4\xi_s}{(\xi_s+1)^2}\right)\Bigg] - \frac{(\xi_t^2+1)}{2\xi_t}\Bigg[\log^2\left(\frac{\xi_t+1}{\xi_t-1}\right) - \log\left(\frac{\xi_t+1}{\xi_t-1}\right) + \mathrm{Li}_2\left(\frac{4\xi_t}{(\xi_t+1)^2}\right)\Bigg] - \frac{(\xi^2_{u_0}+1)}{2\xi_{u_0}}\Bigg[\log^2\left(\frac{\xi_{u_0}+1}{\xi_{u_0}-1}\right) - \log\left(\frac{\xi_{u_0}+1}{\xi_{u_0}-1}\right) + \mathrm{Li}_2\left(\frac{4\xi_{u_0}}{(\xi_{u_0}+1)^2}\right)\Bigg] - S_\phi(-(\xi^2_{u0}+1)u_0, (\xi_s^2+1)s, -(\xi_t^2+1)t) + S_\phi(-(\xi^2_{u0}+1)u_0, -(\xi_t^2+1)t, (\xi_s^2+1)s) - S_\phi(-(\xi_t^2+1)t, (\xi_s^2+1)s, -(\xi^2_{u0}+1)u_0) + 1 \quad (71)$$

with

$$H(s) = \frac{\xi_s^2+1}{2\xi_s}\Bigg[\mathrm{Li}_2\left(\frac{z_s}{z_1}\right) + \mathrm{Li}_2\left(\frac{z_s}{z_2}\right) - \mathrm{Li}_2\left(\frac{z_s}{z_3}\right) - \mathrm{Li}_2\left(\frac{z_s}{z_4}\right) - \log\left(\frac{(\xi_s+1)^2}{(\xi_s-1)^2}\right)\log\left(\frac{(z_s-1)^2 - \xi_s^2}{1-\xi_s^2}\right)\Bigg] \quad (72)$$

$$v_{max} = \frac{st + \sqrt{s(s-4m^2)t(t-4m^2)}}{2m^2} \quad (73)$$

$$z_{u1} = \frac{\sqrt{v_{max} - \xi^2_{u0}(v_{max}+u_0)}}{\xi_{u0}\sqrt{-u_0}} \quad (74)$$

$$z_{u2} = \frac{1}{\xi_{u0}}\sqrt{\frac{v_{max} + \xi^2_{u0}u_0}{v_{max}+u_0}} \quad (75)$$

$$z_s = \frac{\xi_s(\sqrt{\xi_s^2 s^2 - 2sv_{max} + v^2_{max}} - \xi_s s)}{v_{max}} + 1 \quad (76)$$

$$z_1 = 1 + \xi_s \quad (77)$$

$$z_2 = \frac{(1+\xi_s)^2}{1-\xi_s} \quad (78)$$

$$z_3 = 1 - \xi_s \quad (79)$$

$$z_4 = \frac{(1-\xi_s)^2}{1+\xi_s} \quad (80)$$

The S_ϕ function is defined as:

$$S_\phi(s_1,s_2,s_3) = \frac{s_3}{2\sqrt{\lambda_3}}\Bigg\{\log\frac{s_2-\sqrt{\lambda_2}}{s_2+\sqrt{\lambda_2}}\log\frac{(z-z_1)(z-z_3)}{(z-z_2)(z-z_4)} + \sum_{i,j}^{4} S_j(-1)^{i+1}\Bigg(\frac{1}{2}\delta_{ij}\log(z-z_i)^2 + (1-\delta_{ij})\Bigg[\log(z-z_i)\log(z_i-z_j) - \mathrm{Li}_2\frac{z-z_i}{z_j-z_i}\Bigg]\Bigg)\Bigg\}\Bigg|_{z=z_d}^{z=z_u} \quad (81)$$

where

$$
\begin{aligned}
z_{1,2} &= \frac{1}{\sqrt{\lambda_2}}\left(\frac{4m^2(s_3 \mp \sqrt{\lambda_3})}{s_2 - \sqrt{\lambda_2}} - s_1 - \sqrt{\lambda_2}\right)\\
z_{3,4} &= \frac{1}{\sqrt{\lambda_2}}\left(s_1 - \sqrt{\lambda_2} - \frac{4m^2(s_3 \pm \sqrt{\lambda_3})}{s_2 + \sqrt{\lambda_2}}\right)\\
z_u &= \frac{\sqrt{\lambda_1}}{\sqrt{\lambda_2}} - 1\\
z_d &= \frac{s_1 s_2 - 4m^2 s_3}{\lambda_2} - 1\\
\lambda_i &= s_i^2 - 16m^4\\
s_j &= (1, 1, -1, -1)
\end{aligned}
\tag{82}
$$

Note that $S_\phi(s_1, s_2, s_3) \equiv S_\phi(s_2, s_1, s_3)$

References

1. L.N. Hand, D.G. Miller, R.Wilson, Rev. Mod. Phys., **35** 335 (1963).
2. G.G. Simon *et al.*, Nucl. Phys., **A333** 381 (1980).
3. P.J. Mohr, B.N. Taylor, D.B. Newell, Rev. Mod. Phys., **80** 633 (2008).
4. K. Melnikov and T. van Ritbergen, Phys. Rev. Lett., **84** 1673 (2000).
5. R. Pohl *et al.*, Nature, **466** 213 (2010).
6. I. Sick, Phys. Lett. B, **576** 62 (2003).
7. Th. Udem, A. Huber, B. Gross, J. Reichert, M. Prevedelli, M. Weitz, T.W. Hänsch, Phys. Rev. Lett., **79** 2646 (1997).
8. K. Melnikov and T. van Ritbergen, Phys. Rev. Lett., **8** 1673 (2000).
9. A. Antognini *et al.*, Science **339** 417 (2013).
10. J. C. Bernauer *et al.*, Phys. Rev. Lett. **105** 242001 (2010).
11. X. Zhan *et al.*, Phys. Lett. B, **705** 59 (2011).
12. K.M. Graczyk, C. Juszczak, ArXiv e-prints, 1408.0150 (2014).
13. I.T. Lorenz, U.-G. Meißner, Phys. Lett. B **737** 57 (2014).
14. I.T. Lorenz, H.W. Hammer, U.-G. Meißner, Eur. Phys. J. A **48** 151 (2012).
15. J. D. Carroll, A. W. Thomas, J. Rafelski, G. A. Miller, AIP Conf. Proc. **1354** 25 (2011).
16. A. De Rujula. Phys. Lett. B, **693** 555 (2010).
17. A. De Rujula, Phys. Lett. B, **697** 26 (2011).
18. B.Y. Wu, C.W. Kao, ArXiv e-prints, 1108.2968 (2011).
19. G.Paz, AIP Conf. Proc. **1441**, 146 (2012).
20. C. Peset, A. Pineda, ArXiv e-prints, 1403.3408 (2014).
21. D. Tucker-Smith I. Yavin, Phys. Rev. D, **83** 101702 (2011).
22. V. Barger, C.W. Chiang, W.Y. Keung, D. Marfatia, Phys. Rev. Lett. **106** 153001 (2011).
23. C.E. Carlson, B.C. Rislow, Phys. Rev. D, **86** 035013 (2012).
24. J. Jaeckel and R. Sabyasachi, Phys. Rev. D, **8** 125020 (2010).
25. Batell et al., Phys. Rev. Lett. **107** 011803 (2011).
26. E. Kraus *et al.*, ArXiv e-prints, 1405.4735 (2014).
27. H. Gao, Int. J. Mod. Phys. E **12** 1 (2003).
28. C.F. Perdrisat, V. Punjabi, M. Vanderhaeghen, Prog. Part. Nucl. Phys. **59** 694 (2007).
29. Jefferson Laboratory Experiment E12-11-106, Spokespersons: A Gasparian (contact), D. Dutta, H. Gao, M. Khandaker, 2011.
30. The PrimEx Collaboration. PrimEx Conceptual Design Report. 2000.
31. I. Bernauer, M. Distler, private communication.
32. R. Gilman *et al.*, ArXiv e-prints, 1303.2160v3 (2013).
33. A. Afanasev, I. Akushevich, and N. Merenkov, Phys. Rev. D **64** 113009 (2001).
34. I. Akushevich, O.F. Filoti, A. Ilyichev, N. Shumeiko, Comput. Phys. Commun. **183** 1448 (2012).
35. A. Ilyichev and V. Zykunov, Phys. Rev. D, **72** 033018 (2005).
36. N. Kaiser, J. Phys. G: Nucl. Part. Phys. **37** 115005 (2010).
37. L.C.. Maximon and J.A Tjon, Phys. Rev. C, **62** 054320 (2000)
38. N.M. Shumeiko and J.G. Suarez, J. Phys. G, **26** 113-127 (2000).
39. D.Y. Bardin, N.M. Shumeiko, Nucl. Phys. B **127** 242 (1977).
40. N.M. Shumeiko, Yad. Fiz., **29** 1571 (1979).
41. M. Bohm, H. Spiesberger, W. Hollik, Fortsch.Phys. **34** 687 (1986).
42. H. Burkhardt, B. Pietrzyk, Phys. Lett. **B356** 398 (1995).
43. A. Afanasev, E. Chudakov, A. Ilyichev, V. Zykunov, Comput. Phys. Commun. **176** 218 (2007).
44. D.M. Nikolenko *et al.*, EPJ Web of Conferences, **66** 06002 (2014).
45. M. Moteabbed *et al.*, Phys. Rev. C, **88** 025210 (2013).
46. M. Kohl *et al.*, EPJ Web of Conferences, **66** 06009 (2014).